Generation of cord blood endothelial colony forming cell–like cells from human pluripotent stem cells

Nutan Prasain[1]*, Man Ryul Lee[2]*, Sasidhar Vemula[1], Jonathan Luke Meador[1], Momoko Yoshimoto[1], Michael J. Ferkowicz[1], Alexa Fett[1], Manav Gupta[1], Brian M. Rapp[3], Mohammad Reza Saadatzadeh[3], Michael Ginsberg[4], Olivier Elemento[5], Younghee Lee[6], Sherry L. Voytik-Harbin[7], Hyung Min Chung[8], Ki Sung Hong[9], Emma Reid[10], Christina L. O'Neill[10], Reinhold J. Medina[10], Alan W. Stitt[10], Michael P. Murphy[3], Shahin Rafii[4], Hal E. Broxmeyer[2], and Mervin C. Yoder[1]**.**

We differentiated hES or hiPS cells in OP9 co-cultures[18] or under EB conditions[17] for 1 week and then expanded cells in endothelial media (**Supplementary Figs. 1a and 2a**) to search for cells with CB-ECFC properties (clonal high proliferative potential and robust *in vivo* vessel forming ability). Early passage cells (passage [P]1) displayed some features of endothelium but, by P4, the cultures became predominantly comprised of cells with a fibroblastic appearance (**Supplementary Figs. 1a and 2a**) and a heterogeneous pattern of CD31, CD144, and CD146 expression (**Supplementary Figs. 1b and 2b**). When plated on Matrigel, cells either formed vascular-like networks with a few large branches (Supplementary Fig. 1c) or vascular-like networks with numerous smaller incomplete sprout-like branches (**Supplementary Fig. 2c**). At P3 or P4, we plated single cells for clonal proliferative potential analysis and scored the outcomes as single cells that did not divide or divided to form colonies of 2-50 (ECFC clusters), 51-500 (low proliferative potential ECFC; LPP-ECFC), 501-2000 (LPP-ECFC), or ≥2000 cells (high proliferative potential-ECFC; HPP-ECFC) as previously described[4-6]. Less than 2% of the endothelial cells derived from OP9 co-cultures or EB-derived cells gave rise to HPP-ECFCs. In fact, most of the OP9 co-culture derived or EB-derived endothelial cells did not divide or gave rise

to ECFC clusters (**Supplementary Figs. 1d and 2d**). These patterns of ECFC colony formation were significantly different from the pattern displayed by single endothelial cells derived from CB-ECFCs, which primarily gave rise to HPP-ECFC or LPP-ECFC and rare clusters (**Supplementary Figs. 1d and 2d**). We were unable to expand the OP9 co-culture– derived or EB-derived endothelial cells beyond P7 due to replicative senescence (data not shown), and the endothelial cells at P5 failed to give rise to human blood vessels *in vivo* upon implantation (**Supplementary Figs. 1e and 2e**).

Next we tested a more recent 2 step endothelial differentiation protocol that involves initial EB formation and then 2D adherent cell culture (with added growth factors and TGFβ inhibitor)[19]. Given the known importance of the vascular endothelial growth factor (VEGF) signaling pathway in the emergence of endothelial cells during development[24] and during endothelial lineage differentiation of hES cells[17], we used neuropilin-1 (NRP-1) as one of the endothelial markers for identifying putative ECFCs. NRP-1 is a VEGF co-receptor and Semaphorin 3A binding multifunctional protein that is expressed in various tissues including endothelial cells, vascular smooth muscle cells and lymphocytes[24]. While the role of NRP-1 in vasculogenesis is unknown, a double knock out of NRP-1 and NRP-2 in mice leads to an embryonic lethal phenotype similar to that of the VEGFR-2 knockout[24]. We generated hES (H9 line) and hiPS cell-derived (DF19-9-11T, FCB-iPS-1 and FCB-iPS-2) EBs in suspension culture for 4 days, and seeded them on Matrigel coated dishes for 10 days[19] (**Supplementary Fig. 3a,b**). Cells co-expressing NRP-1 and CD31 (NRP-1$^+$CD31$^+$ cells) appeared on day 3 (0.17%) and increased overtime to peak at day 14 (1.6%) (**Supplementary Fig. 3c**). The different subsets of sorted cells were subsequently cultured in endothelial growth (EGM-2) media supplemented with TGFβ inhibitor (10 μM SB431542) for 2 weeks as described[19], as TGFβ inhibition has been reported to promote endothelial lineage differentiation from hES or hiPS cells and to prevent the cells from transitioning

to a mesenchymal fate. While most hES-derived cell subsets formed incomplete capillary networks upon plating in Matrigel, NRP-1^{+}CD31^{+} cells formed complete structures similar to those exhibited by CB derived ECFCs (**Supplementary Fig. 3d**). At a clonal level, all of the individual NRP-1^{+}CD31^{+} plated cells divided and many clones (37%) formed HPP-ECFC, while few NRP-1^{+}CD31^{-} or NRP-1^{-}CD31^{+} cells formed HPP-ECFC (**Supplementary Fig. 3e**). Thus, co-expression of NRP-1 and CD31 in hES-derived cells undergoing endothelial differentiation (EB plus 2D protocol) identified a progenitor subset that gave rise to endothelial cells with high clonal proliferative potential and angiogenic activity, but only if cultured in the continual presence of TGF-β inhibition. Removal of the inhibitor was associated with diminished proliferative potential, loss of endothelial morphology, and increased expression of alpha-smooth muscle actin [α-SMA] as previously described[19, 23]. Thus, all of the tested methods did not generate stable endothelial cells with CB-ECFC properties.

Human iPS-Day 0 cells displayed a transcriptome profile characteristic of pluripotent cells with limited expression of transcripts typically seen in differentiated cells (**Supplementary Fig. 7a**). However, hiPS-Day 3 cells displayed increased expression for multiple lineage specific genes (primitive streak, endoderm, mesoderm, hematopoietic, and chondro-osteo-adipogenic genes), indicating initiation of pluripotent cell differentiation (**Supplementary Fig. 7a**).

Supplementary Figure 1: Examination of morphology, endothelial antigen expression, clonal proliferative potential, and *in vitro* and *in vivo* vessel forming potential of endothelial cells derived from hES and hiPS cells differentiated by co-culturing them with OP9 stromal cells.

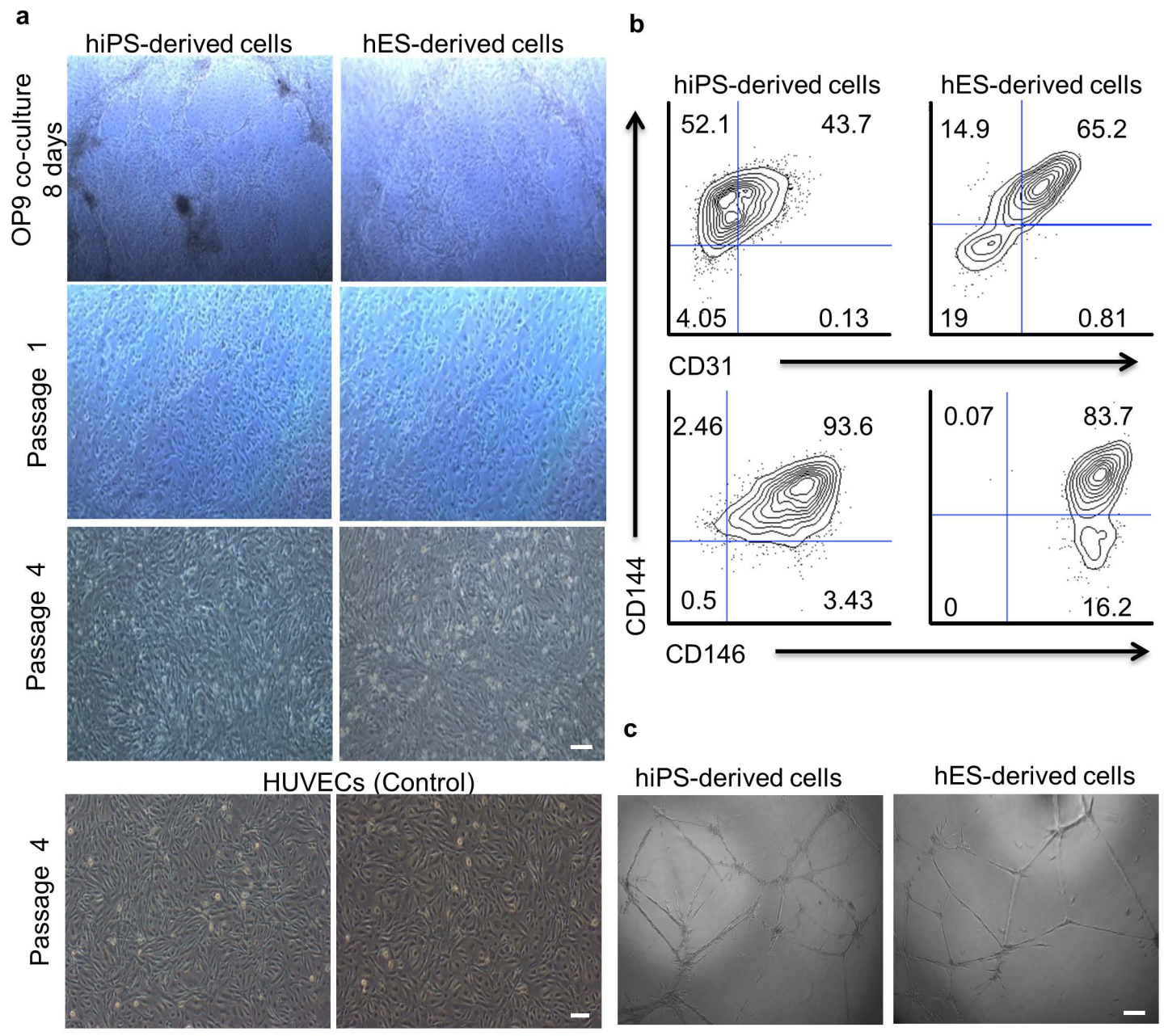

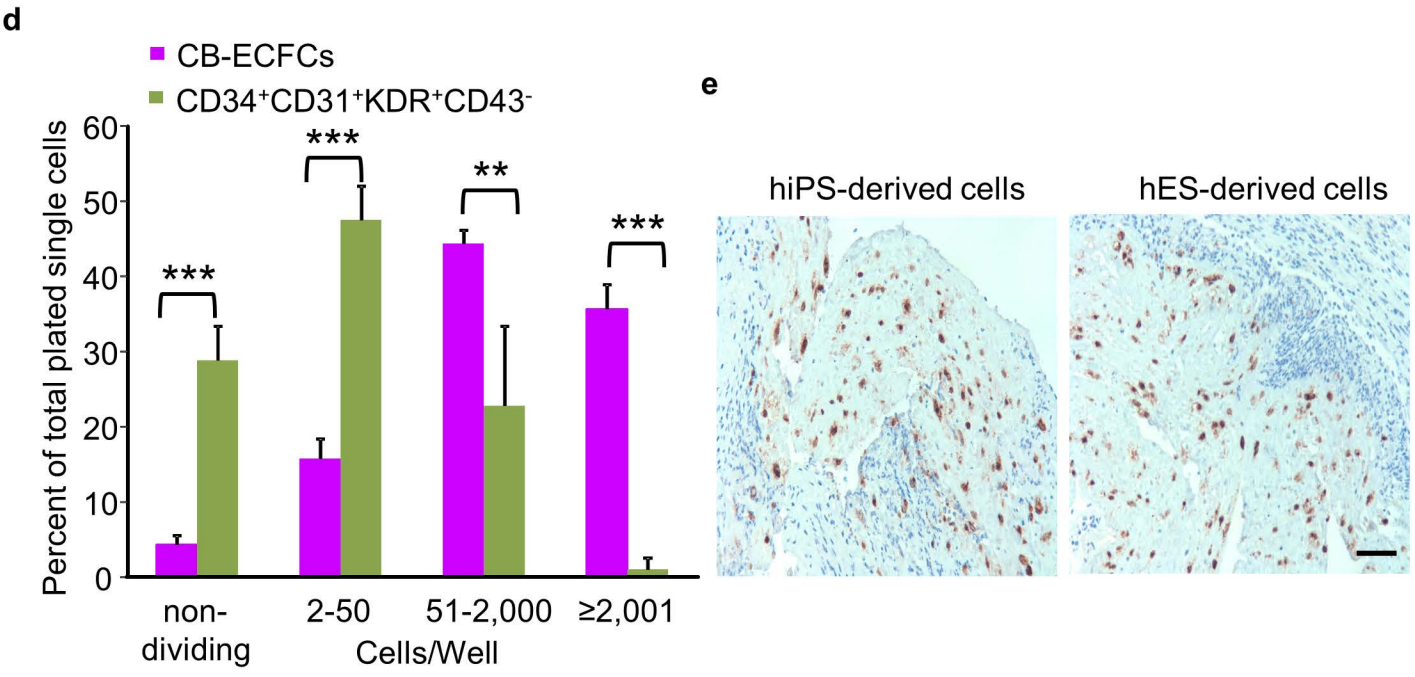

Supplementary Figure 1: Examination of morphology, endothelial antigen expression, clonal proliferative potential, and *in vitro* and *in vivo* vessel forming potential of endothelial cells derived from hES and hiPS cells differentiated by co-culturing them with OP9 stromal cells. (a) Representative phase contrast photomicrographs of hES and hiPS cells at day 8 after undergoing endothelial lineage differentiation in co-culture with OP9 cells (top panels) and culture of isolated cells at P1 and P4 (middle and bottom panels respectively). Differentiated cells at day 8 exhibited areas of cells with endothelial like morphology (top panels). Upon isolation and culture in endothelial culture medium, they initially displayed endothelial cobblestone-like morphology at P1 (middle panels) and progressively become a heterogeneous population of cells with few cells displaying an endothelial cobblestone morphology by P4. Representative phase contrast photomicrographs showing characteristic cobblestone endothelial phenotype in human umbilical vein endothelial cells (HUVECs). All experiments were performed 5 times in duplicates and a representative photomicrograph is shown for each group. Scale bars, 100 µm. **(b)** Human iPS and hES-derived cells (P4) obtained from co-culturing cells with OP9 were stained with monoclonal antibodies against human CD31, CD144 and CD146. Percentages in the top panel contour plots indicates CD144 and CD31 double positive cells, percentages in the bottom panel contour plots indicates CD144 and CD146 double positive cells. In both hiPS and hES derived cells, a heterogeneous pattern of CD31, CD144 and CD146 expression was exhibited with only a portion of the cells expressing each of these antigens. All experiments were performed 4 times in duplicates and a representative contour plot is shown for each group. **(c)** Representative photomicrographs of OP9 co-cultured hiPS and hES-derived cells (P4) shown to form a few large branches of capillary-like networks on Matrigel. All experiments were performed 5 times in duplicates and a representative photomicrograph is shown for each group. Scale bar, 100 µm. **(d)** A bar graph depicts the clonal proliferative analysis of OP9 co-cultured hES-derived cells (P3 to 4) in comparison with a CB-ECFC control. The distribution pattern of HPP-ECFC and LPP-ECFC colonies formed by OP9 co-cultured hES-derived cloned cells is significantly different to the distribution pattern displayed by CB-ECFC clones. n = 3; mean ± SD. Student's *t*-test: $^{**}p<0.01$ and $^{***}p<0.001$. **(e)** Representative photomicrographs of OP9 co-cultured hiPS and hES-derived cells (P4) that failed to form mouse red blood cell filled functional human vessels *in vivo* upon implantation. All experiments were performed 5 times in duplicates and a representative photomicrograph is shown for each group. Scale bar, 100 µm.

Supplementary Figure 2: Examination of morphology, endothelial antigen expression, clonal proliferative potential, and *in vitro* and *in vivo* vessel forming potential of endothelial cells obtained from EB-mediated endothelial lineage differentiation of hES and hiPS cells.

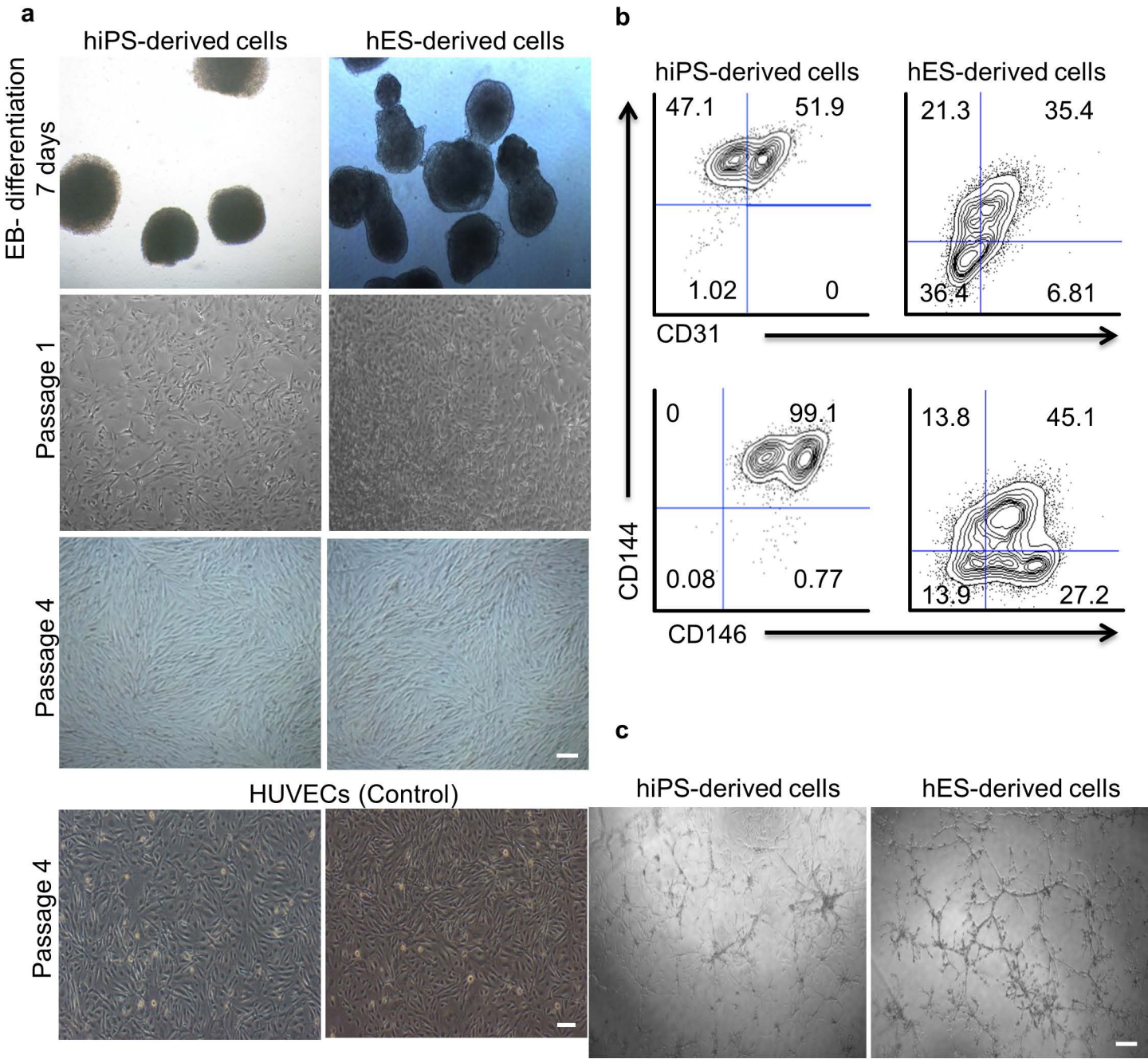

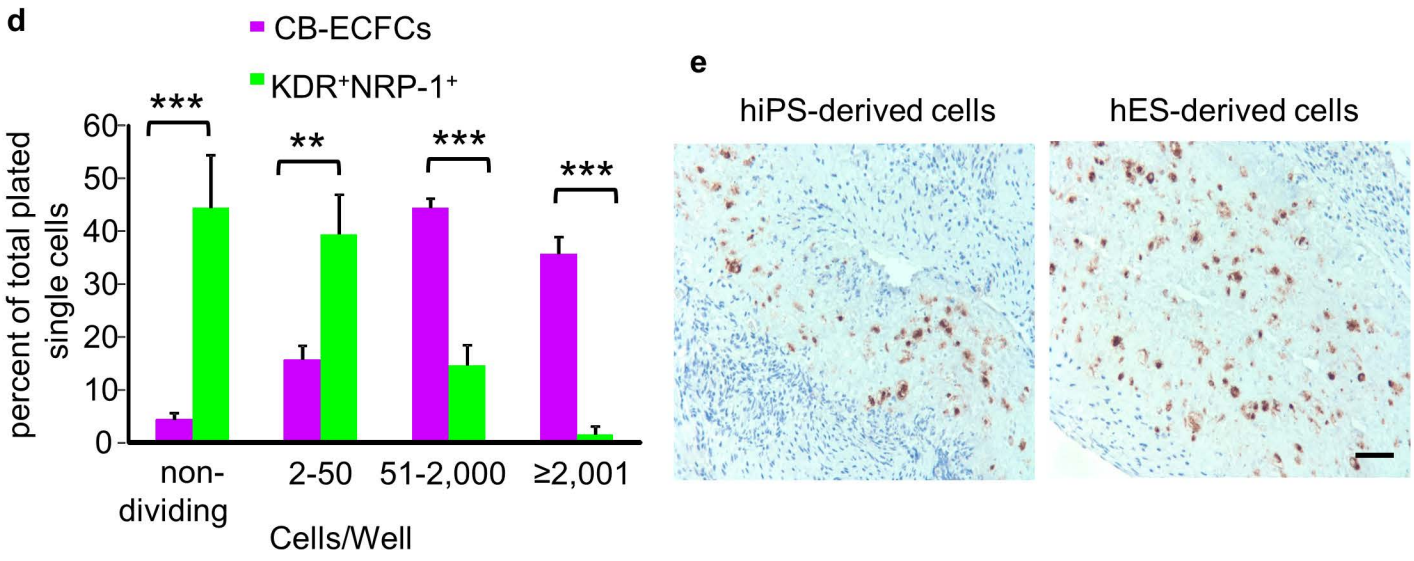

Supplementary Figure 2: Examination of morphology, endothelial antigen expression, clonal proliferative potential, and *in vitro* and *in vivo* vessel forming potential of endothelial cells obtained from EB-mediated endothelial lineage differentiation of hES and hiPS cells. (a) Representative phase contrast photomicrographs of hES and hiPS cell-derived EBs at day 7 of EB-mediated endothelial lineage differentiation (top panels) and culture of isolated cells at P1 and P4 (middle and bottom panels, respectively). $KDR^{+}NRP\text{-}1^{+}$ cells upon isolation and culture in endothelial culture medium displayed a heterogeneous population of cell morphologies, where only a portion of cells displayed endothelial features (middle panels). Upon further expansion (P4) these cells became predominantly comprised of cells with fibroblastic-like appearance and little endothelial cobblestone morphology (bottom panels). Representative phase contrast photomicrographs showing characteristic cobblestone endothelial phenotype in human umbilical vein endothelial cells (HUVECs). All experiments were performed 5 times in duplicates and a representative photomicrograph is shown for each group. Scale bars, 100 μm. **(b)** Human iPS and hES-derived cells (P4) obtained from the EB-based protocol were stained with monoclonal antibodies against human CD31, CD144 and CD146. Percentages in top panel contour plots depict CD144 and CD31 double positive cells and percentages in the bottom panel contour plots indicate CD144 and CD146 double positive cells. In both hiPS and hES derived cells, a heterogeneous pattern of CD31, CD144 and CD146 expression was exhibited with only a portion of the cells expressing each of these antigens. All experiments were performed 4 times in duplicates and a representative contour plot is shown for each group. **(c)** Representative photomicrographs of EB-based hiPS and hES-derived cells (P4) that formed capillary-like networks with numerous smaller incomplete branches on Matrigel. All experiments were performed 5 times in duplicates and a representative photomicrograph is shown for each group. Scale bar, 100 μm. **(d)** A bar graph depicting clonal proliferative analysis of EB-based hES-derived cells (P3 to P4) in comparison with CB-ECFC control cells. The distribution pattern of HPP-ECFC and LPP-ECFC derived colonies formed by EB-based hES-derived cells is significantly different to the distribution pattern displayed by the CB-ECFC clones. n = 3; mean ± SD. Student's *t*-test: $^{**}p<0.01$ and $^{***}p<0.001$. **(e)** Representative photomicrographs of EB-based hiPS and hES-derived cells (P4) that failed to form mouse red blood cell filled functional human vessels *in vivo* upon implantation. All experiments were performed 5 times in duplicates and a representative photomicrograph is shown for each group. Scale bar, 100 μm.

Supplementary Figure 3: Examination of morphology, endothelial antigen expression, clonal proliferative potential, and *in vitro* Matrigel network forming potential of endothelial cells obtained from EB plus 2D-based endothelial lineage differentiation of hES cells.

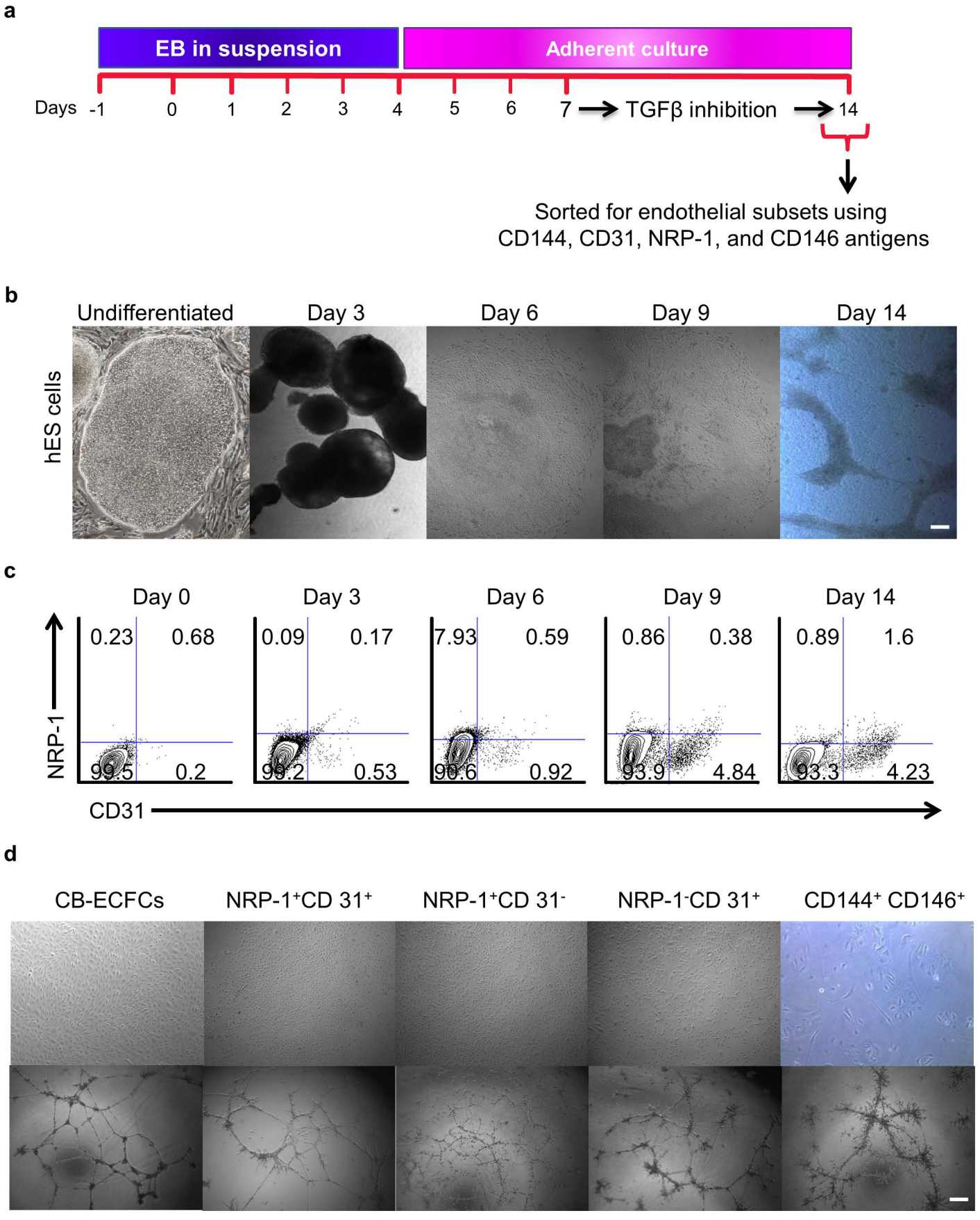

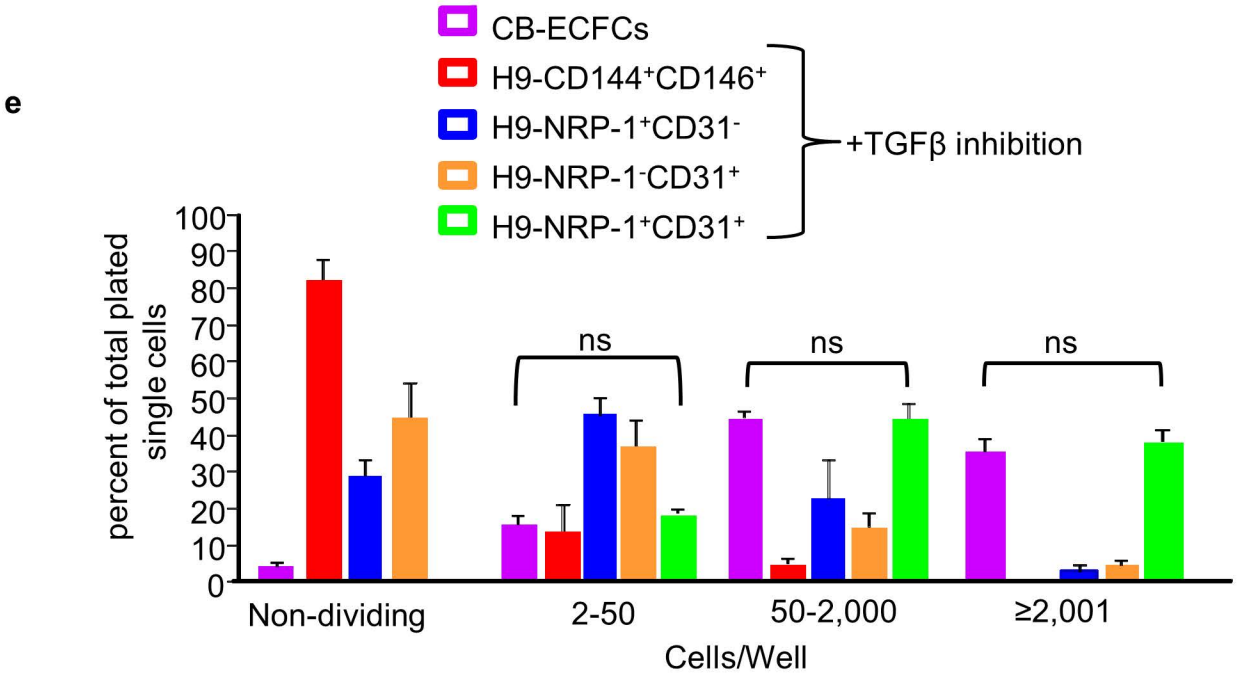

Supplementary Figure 3: Examination of morphology, endothelial antigen expression, clonal proliferative potential, and *in vitro* Matrigel network forming potential of endothelial cells obtained from EB plus 2D-based endothelial lineage differentiation of hES cells. **(a)** Schematic representation of endothelial lineage differentiation of hES cells in EB plus 2D-based differentiation protocol as previously described[19]. This protocol requires continuous exposure of the differentiating endothelial cells to TGFβ inhibition starting at day 7 as indicated. **(b)** Representative phase contrast photomicrographs of hES cells undergoing endothelial lineage differentiation at different days in EB plus 2D-based differentiation protocol. When EBs (2nd panel from left) were attached to Matrigel coated plates at day 4, EB-derived cells in 2D culture adhered and grew to form areas of cells with endothelial-like morphology (at days 6 and 9) and became confluent by day 14. All experiments were performed 5 times in duplicates and a representative photomicrograph is shown for each group. Scale bar, 100 μm. **(c)** Representative contour plots of hES cells undergoing endothelial lineage differentiation at different days in the EB plus 2D-based differentiation protocol. Cells were stained with monoclonal antibodies against various human endothelial antigens at different time points while undergoing 14 days of endothelial lineage differentiation. Percentages in contour plots indicate NRP-1 and CD31 double positive cells. Cells co-expressing NRP-1 and CD31 (NRP-1$^+$CD31$^+$ cells) appeared on day 3 (0.17%) and increased overtime to peak at day 14 (1.6%). All experiments were performed 5 times in duplicates and a representative photomicrograph is shown for each group. **(d)** Representative phase contrast photomicrographs of different subsets (NRP-1$^+$CD31$^+$, NRP-1$^+$CD31$^-$, NRP-1$^-$CD31$^+$ and CD144$^+$CD146$^+$) of sorted cells derived at day 14 from hES cells undergoing endothelial lineage differentiation in the EB plus 2D-based differentiation protocol. The NRP-1$^+$CD31$^+$ subset gave rise to cells with a characteristic endothelial cobblestone morphology similar to that displayed by CB-ECFCs (top panels). While most hES-derived subsets formed incomplete capillary-like networks upon plating on Matrigel, NRP-1$^+$CD31$^+$ cells formed complete capillary-like networks similar to those exhibited by CB derived ECFC control (bottom panels). All experiments were performed 5 times in duplicates and a representative photomicrograph is shown for each group. Scale bar, 100 μm. **(e)** A bar graph depicting the results of a clonal proliferative analysis of EB-2D-based hES-derived various subsets (P3 to P4) in comparison with CB-ECFC control. The distribution pattern of HPP-ECFC and LPP-ECFC colonies formed by NRP-1$^+$CD31$^-$, NRP-1$^-$CD31$^+$ and CD144$^+$CD146$^+$ subsets is significantly different to the pattern displayed by CB-ECFCs. However, the distribution pattern of HPP-ECFC and LPP-ECFC colonies formed by single NRP-1$^+$CD31$^+$ cells was similar to the pattern displayed by CB-ECFC clones. n = 3; mean ± SD. Student's *t*-test: *p* = ns.

Supplementary Figure 4: Human PSC-derived NRP-1$^-$CD31$^+$ cell do not possess ECFC properties.

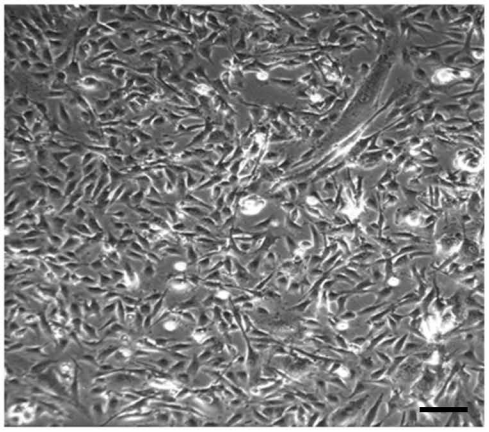

a

NRP-1$^-$CD31$^+$

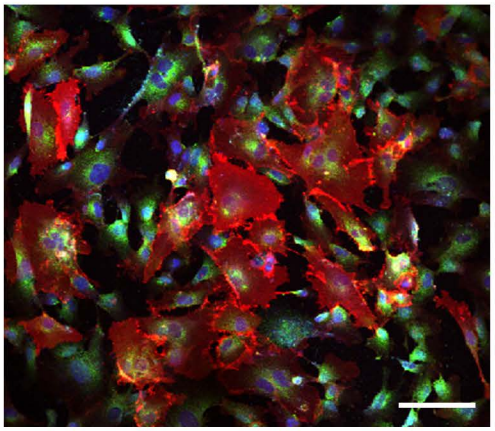

b

NRP-1$^-$CD31$^+$

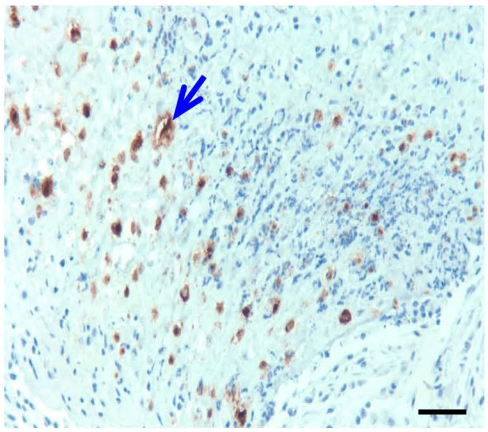

c

NRP-1$^-$CD31$^+$

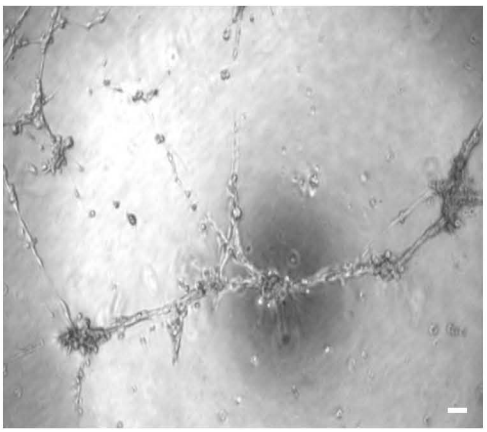

d

NRP-1$^-$CD31$^+$

e

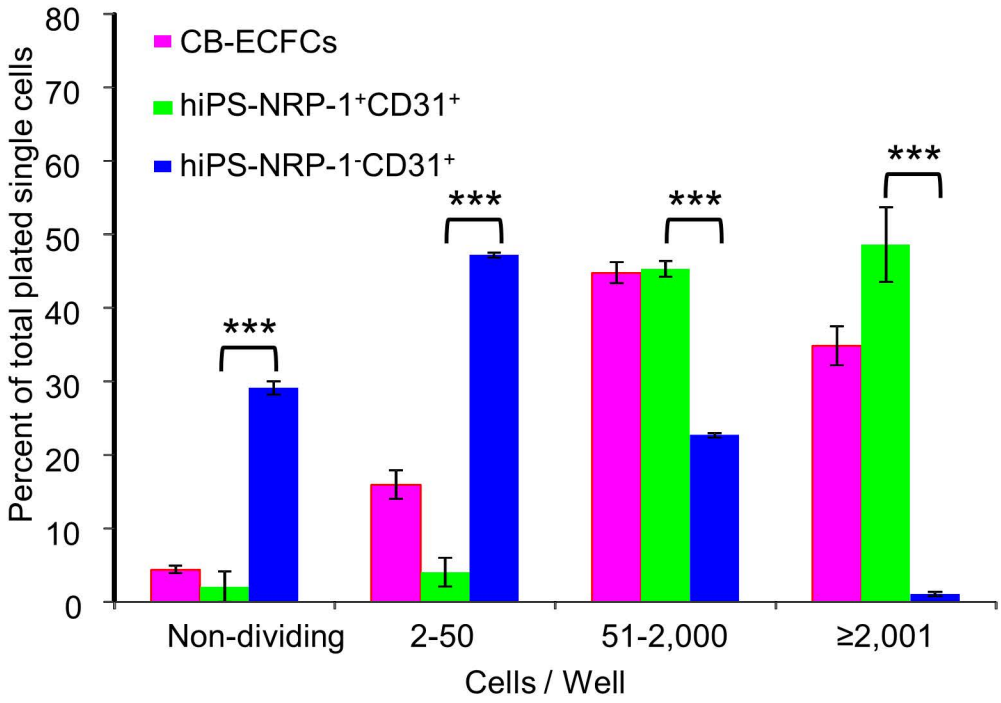

Supplementary Figure 4: Human PSC-derived NRP-1$^-$CD31$^+$ cell do not possess ECFC properties. (a) A representative photomicrograph of an endothelial colony obtained from NRP-1$^-$CD31$^+$ cells exhibiting heterogenous morphologies. Experiments were performed 8 times in duplicates. Scale bar, 100 µm. **(b)** A representative immunofluorescence micrograph of NRP-1$^-$CD31$^+$ cells exhibiting predominant expression of the non-endothelial marker α-SMA with few cells expressing the endothelial surface marker CD144. CD144 expression represented in red; α-SMA expression represented in green; and DAPI was used to stain the nucleus in blue. Experiments were performed 4 times in duplicates. Scale bar, 100 µm. **(c)** A representative photomicrograph of NRP-1$^-$CD31$^+$ cells exhibiting the inability to form murine red blood cell filled functional human vessels *in vivo* upon implantation. Instead, the NRP-1$^-$CD31$^+$ cells formed small lumens with no RBCs (indicated by arrow) suggesting a defect in inosculation. All experiments were performed 5 times in duplicates. Scale bar, 100 µm. **(d)** A representative phase contrast photomicrograph of NRP-1$^-$CD31$^+$ cells exhibiting formation of incomplete capillary-like networks on Matrigel. All experiments were performed 5 times in duplicates. Scale bar, 100 µm. **(e)** A bar graph depicting the results of clonal proliferative analysis of hiPS-derived NRP-1$^-$CD31$^+$ and NRP-1$^+$CD31$^+$ cells in comparison with single plated CB-ECFC control. The distribution pattern of colonies formed by clones of hiPS-NRP-1$^+$CD31$^+$ was similar to the pattern displayed by the CB-ECFC clones. However, the distribution pattern of colonies formed by the hiPS-NRP-1$^-$CD31$^+$ subset is significantly different in comparison with the pattern displayed by both CB-ECFCs and hiPS-NRP-1$^+$CD31$^+$ cells. n = 3; mean ± SD. Student's *t*-test: ***p<0.001.

Supplementary Figure 5: HumaniPSC-ECFCs integrate into the ischemic retinal vasculature *in vivo*.

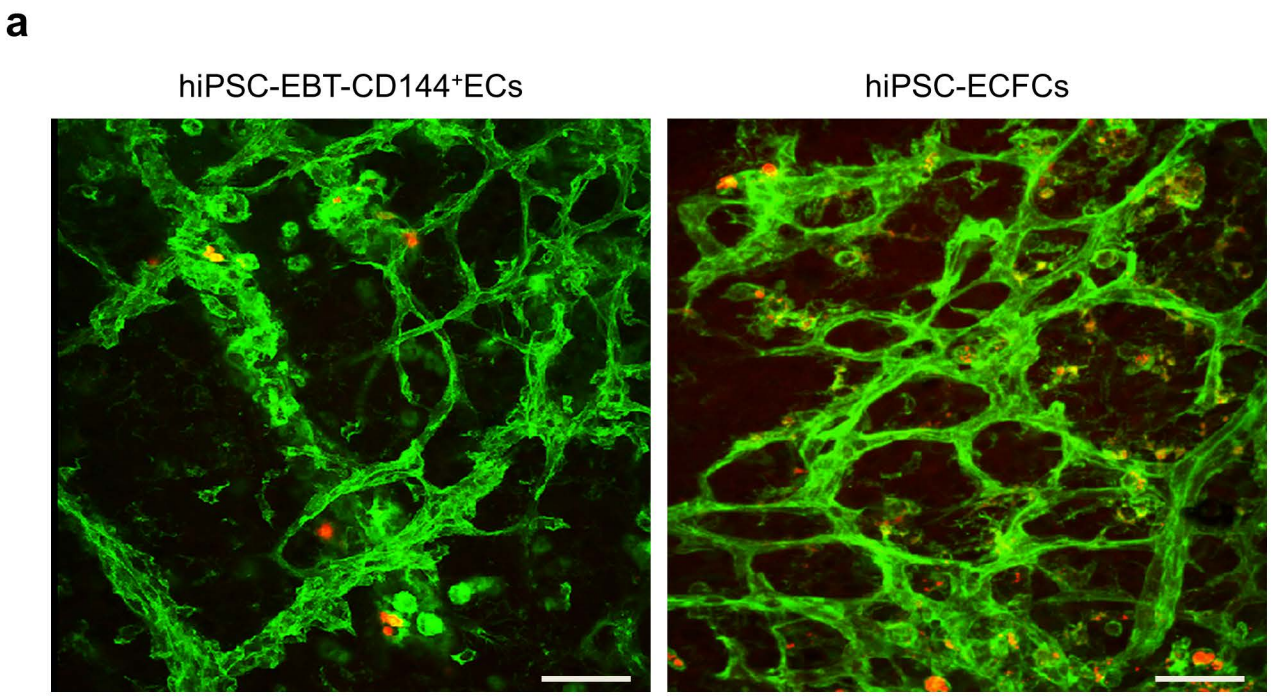

b

hiPSC-ECFCs

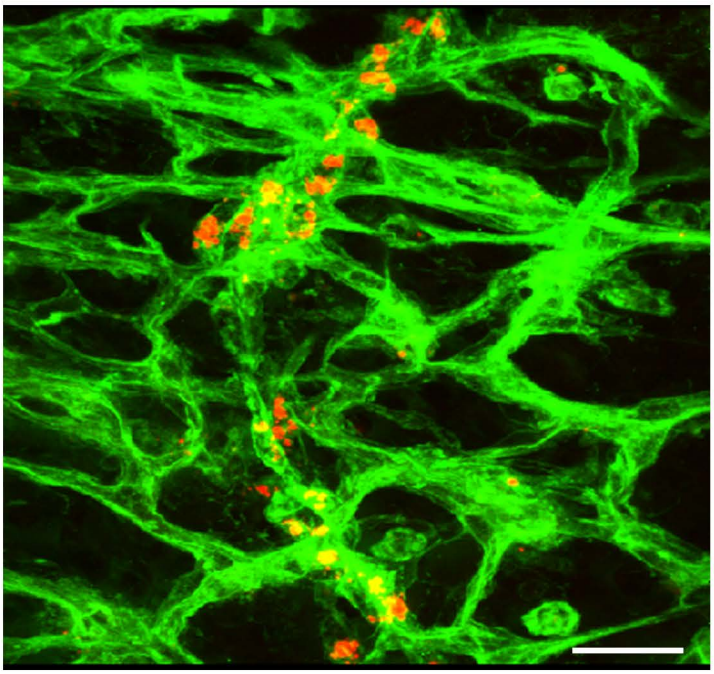

Supplementary Figure 5: HumaniPSC-ECFCs integrate into the ischemic retinal vasculature *in vivo*. (a) HiPSC-ECFCs (top right) or hiPSC-EBT-CD144^{+}ECs (top left) were labeled in red with quantum dots and injected into ischemic retinas subsequently incorporated into the resident vasculature (stained green with isolectin B4). Human iPSC-ECFCs integrate in higher number and wider distribution in host retinas when compared to hiPSC-EBT-CD144^{+}ECs. All experiments were performed ≥4 times. Scale bars, 50 μm. **(b)** Red quantum dot labelled hiPSC-ECFCs are present in close association with host vasculature as single cells and also appear to form vascular tube like structures in the superficial retinal plexus. All experiments were performed ≥4 times. Scale bars, 25 μm.

Supplementary Figure 6: Human PSC-ECFCs undergo extensive expansion, maintain stable endothelial phenotype, and exhibit characteristics of primary cells by ultimately becoming senescent after long term culture.

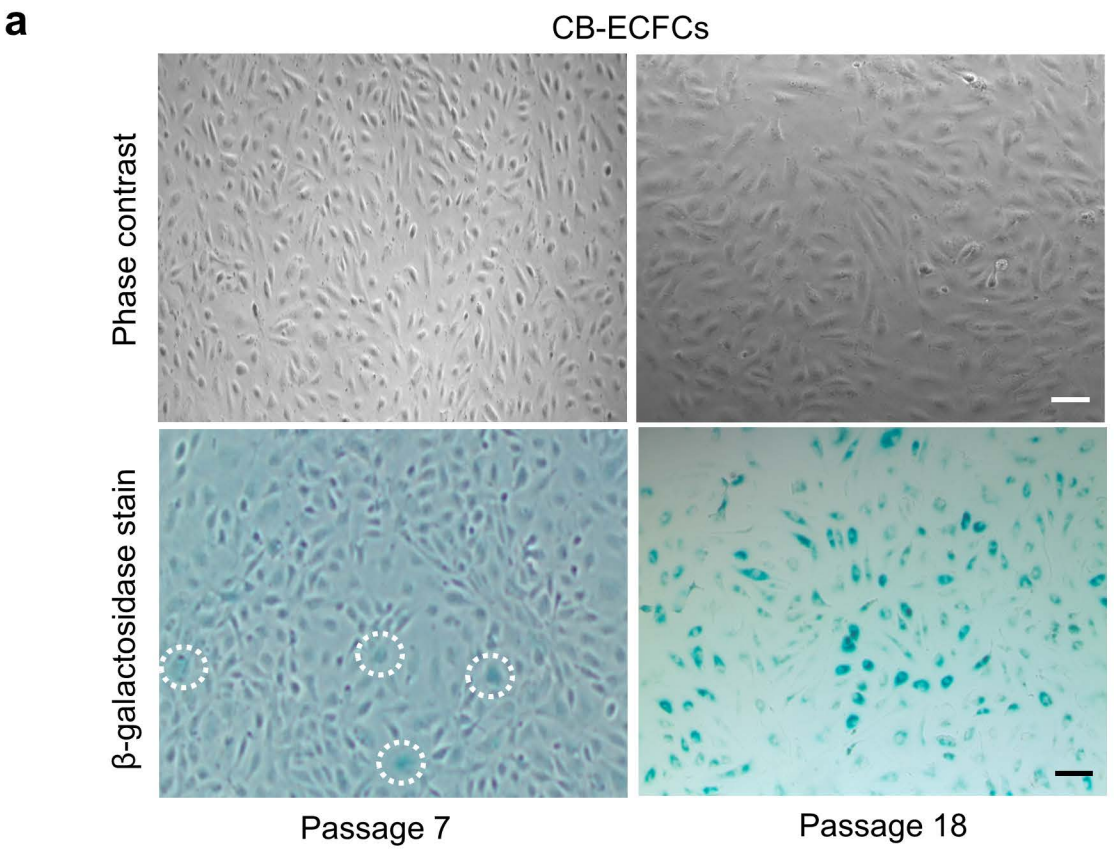

b

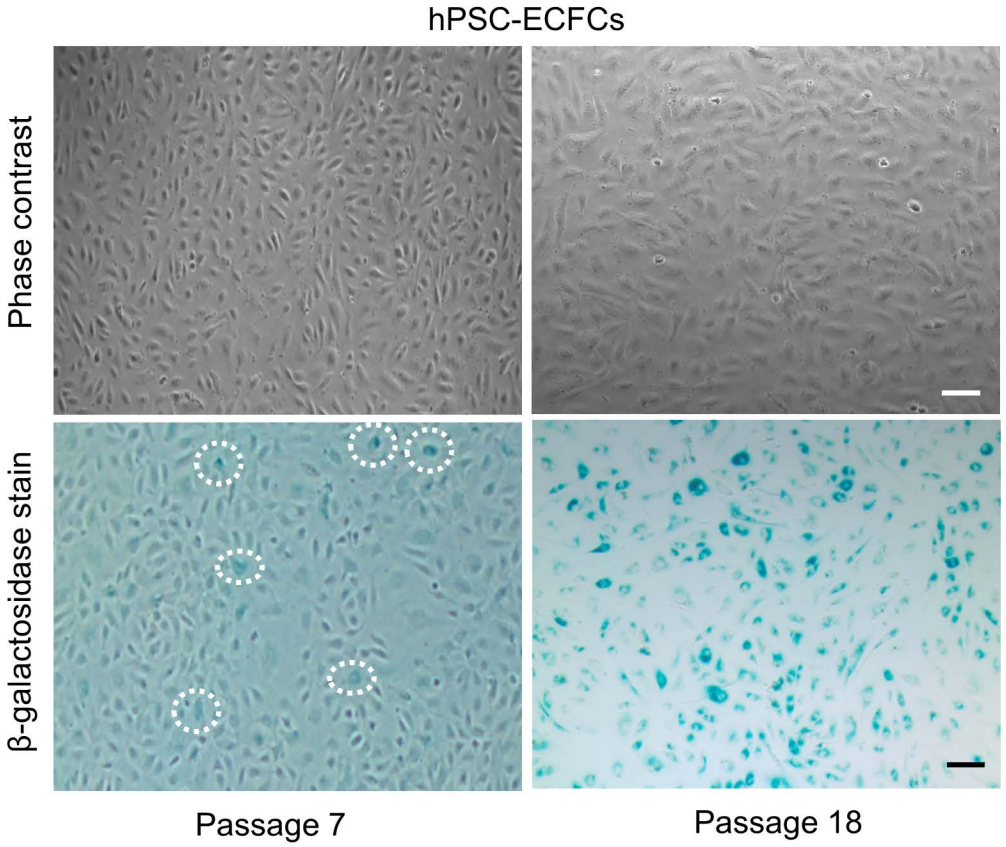
hPSC-ECFCs
Phase contrast
β-galactosidase stain
Passage 7
Passage 18

c

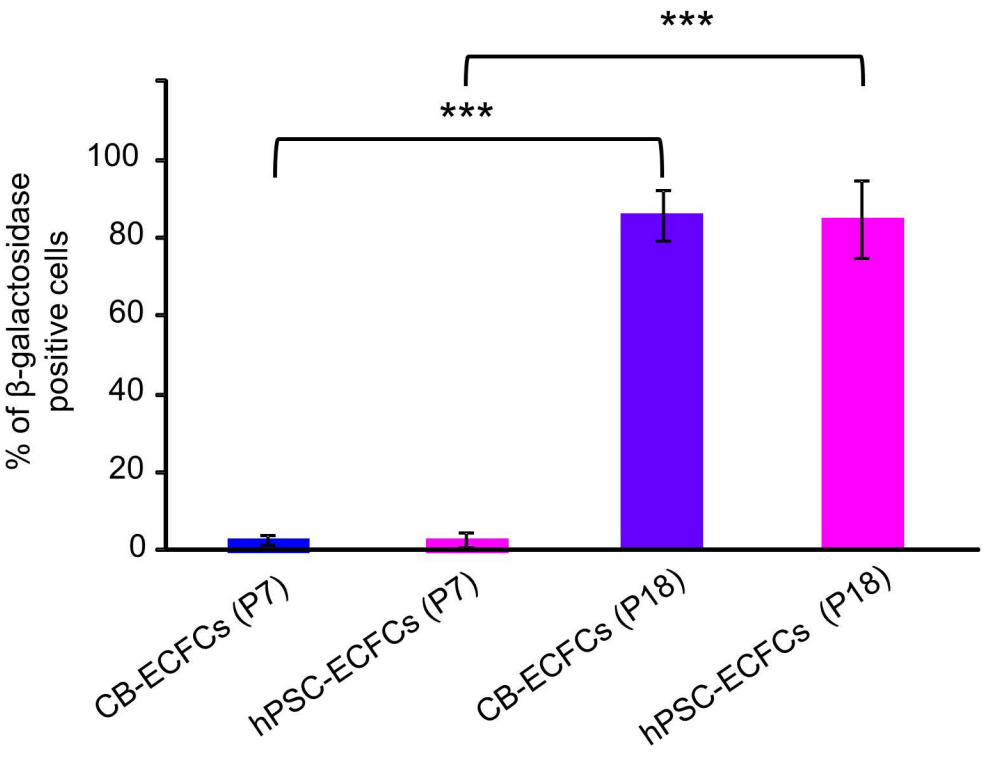
***
***
% of β-galactosidase positive cells
100
80
60
40
20
0
CB-ECFCs (P7)
hPSC-ECFCs (P7)
CB-ECFCs (P18)
hPSC-ECFCs (P18)

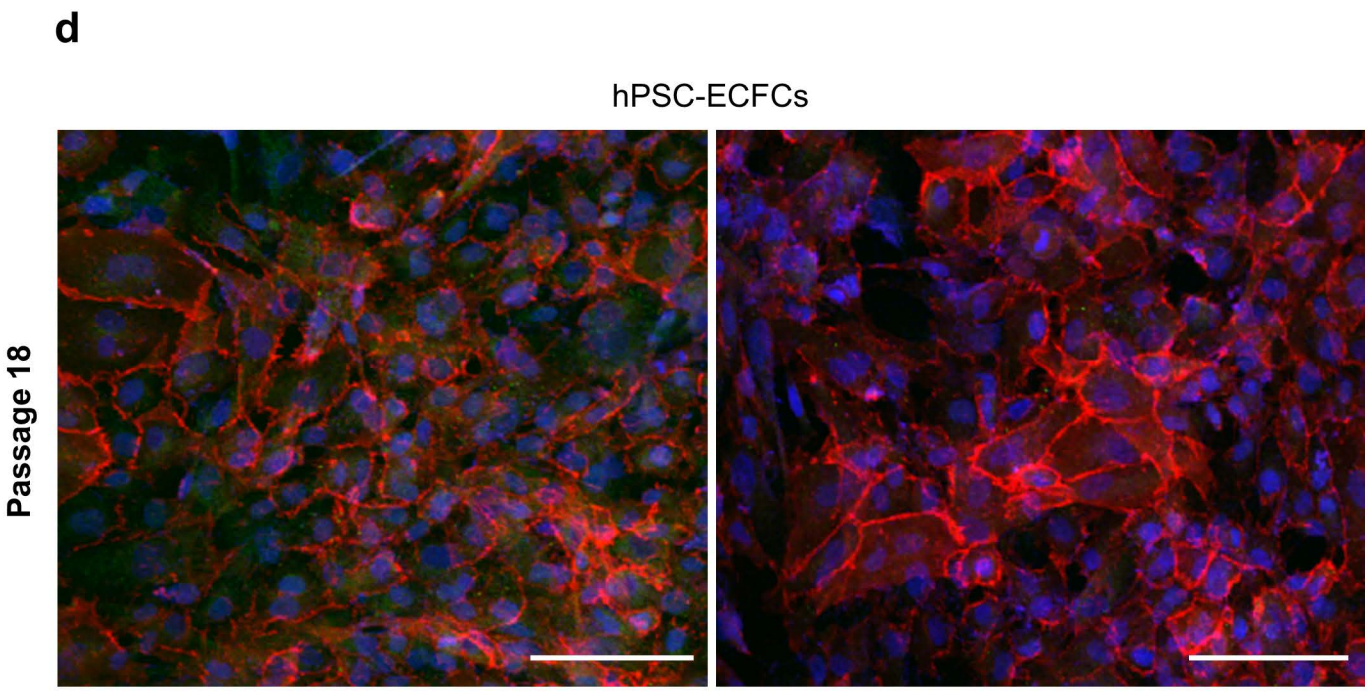

Supplementary Figure 6: Human PSC-ECFCs undergo extensive expansion, maintain stable endothelial phenotype, and exhibit characteristics of primary cells by ultimately becoming senescent after long term culture. (a) Representative phase contrast photomicrographs of CB-ECFCs and hPSC-ECFCs. Human PSC-ECFCs exhibited a homogenous cobblestone endothelial monolayer similar to that of the CB-ECFC control. All experiments were performed 8 times in duplicates and a representative photomicrograph is shown for each group. Scale bar, 50 μm. **(b)** Representative phase contrast photomicrographs of CB-ECFCs and hPSC-ECFCs showing β-galactosidase staining. CB-ECFCs and hPSC-ECFCs were stained with β-galactosidase as per manufacturer's instruction. CB-ECFCs and hPSC-ECFCs were successfully expanded to P18. Both CB-ECFCs and hPSC-ECFCs exhibited few β-galactosidase positive blue cells (indicated by circles) at P7 but by P18 almost all of these cells were positive for β-galactosidase blue staining. All experiments were performed 4 times in duplicates and a representative photomicrograph is shown for each group. Scale bar, 50 μm. **(c)** A bar graph depicting the percentages of β-galactosidase positive cells in CB-ECFCs and hPSC-ECFCs from different passages. Significantly increased percentages of β-galactosidase positive blue cells were observed P18 in both CB-ECFCs and hPSC-ECFCs. n = 10 ; mean ± SD. Student's *t*-test: ***$p<0.001$. **(d)** Representative immunofluorescence micrographs of hPSC-ECFCs displaying expression of the endothelial markers CD31, CD144 and NRP-1 and the non-endothelial marker α-SMA. In left panel, NRP-1 expression represented in green; CD31 expression represented in red. In right panel, α-SMA expression represented in green; CD144 expression represented in red. DAPI was used to stain the nucleus in blue. While CD31, CD144 and NRP1 expression was observed, expression for α-SMA is completely absent in these cells. All experiments were performed 3 times in duplicates and a representative photomicrograph is shown for each group. Scale bars, 100 μm.

Supplementary Figure 7: Human PSC-derived NRP-1^{+}CD31^{+} ECFCs display molecular signatures similar to CB-ECFCs.

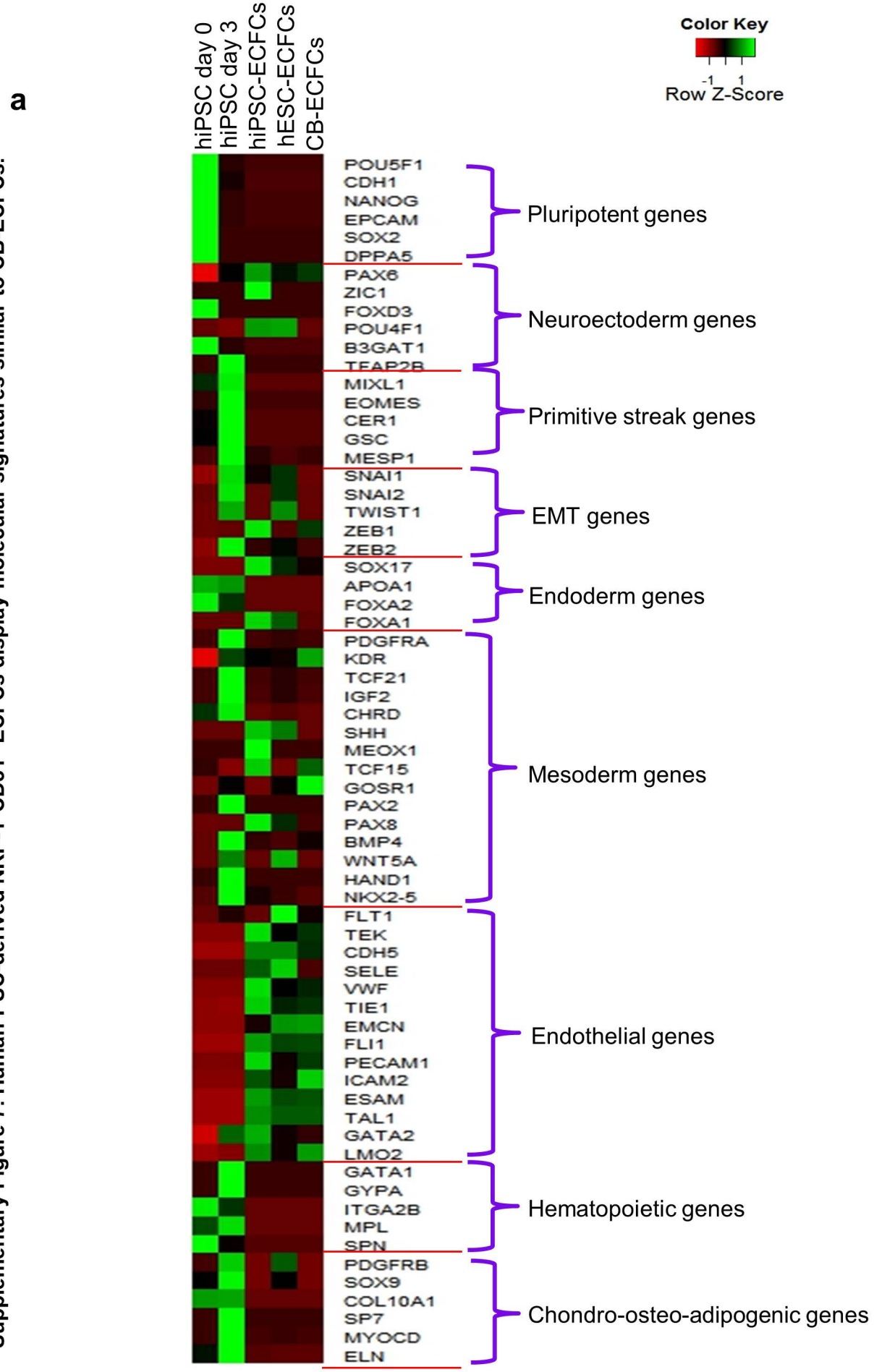

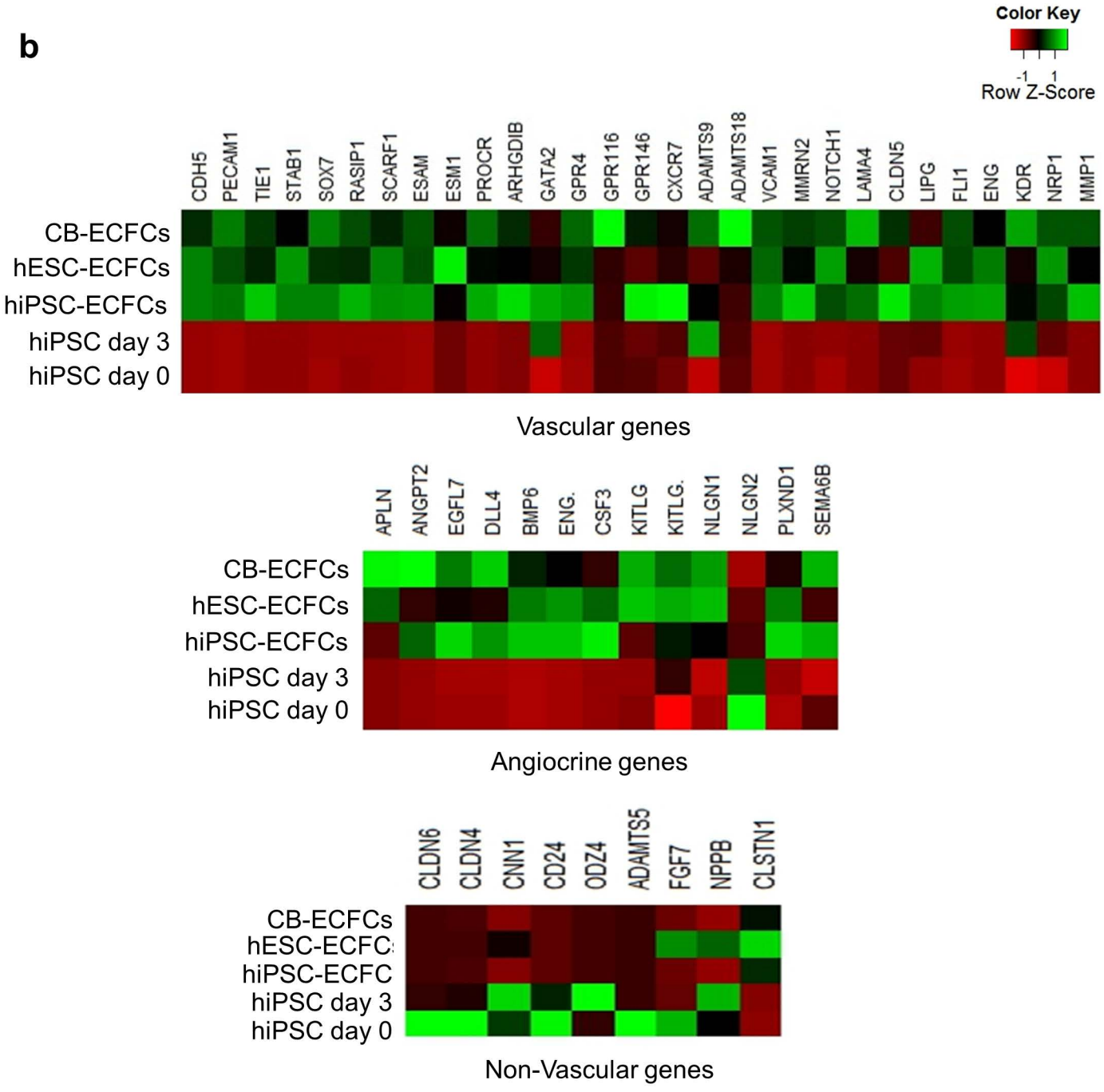

Supplementary Figure 7: Human PSC-derived NRP-1^{+}CD31^{+} ECFCs display molecular signatures similar to CB-ECFCs. (a) Shown is a heatmap of relative transcriptional levels for a select group of genes defining individual germ layers and specific lineages. RNA-sequence analysis was performed on total RNA isolated from hiPS day 0 cells, hiPS day 3 cells, hiPSC-ECFCs, hESC-ECFCs and CB-ECFCs. Select groups of genes belonging to individual germ layer and lineages were analyzed by plotting heatmaps using a red-to-green color scale. Human iPSC-ECFCs and hESC-ECFCs exhibited similar relative gene expression profiles to those displayed by CB-ECFCs. **(b)** Shown are heatmaps of relative transcriptional levels for a select group of vascular, angiocrine, and non-vascular genes as previously described[23]. RNA-sequence analysis was performed on total RNA isolated from hiPS day 0 cells, hiPS day 3 cells, hiPSC-ECFC, hESC-ECFCs and CB-ECFCs. A select group of vascular, angiocrine and non-vascular genes were analyzed by plotting heatmaps using a red-to-green color scale. Human iPSC-ECFCs and hESC-ECFCs exhibited high expression profiles for many vascular (top panel) and angiocrine (middle panel) genes and decreased expression for non-vascular genes (bottom panel), similar to that exhibited by CB-ECFCs.

Supplementary Figure 8 : PAD patients derived ECs possess diminished NRP-1 expression, undergo early cell senescence, fail to exhibit a complete hierarchy of clonal proliferative potential and have deficient *in vivo* vessel forming ability, however, exogenous NRP-1 treatment in PAD ECs decreases cell senescence, reduces multi nuclear cell formation and rescues PAD-EC proliferative potential.

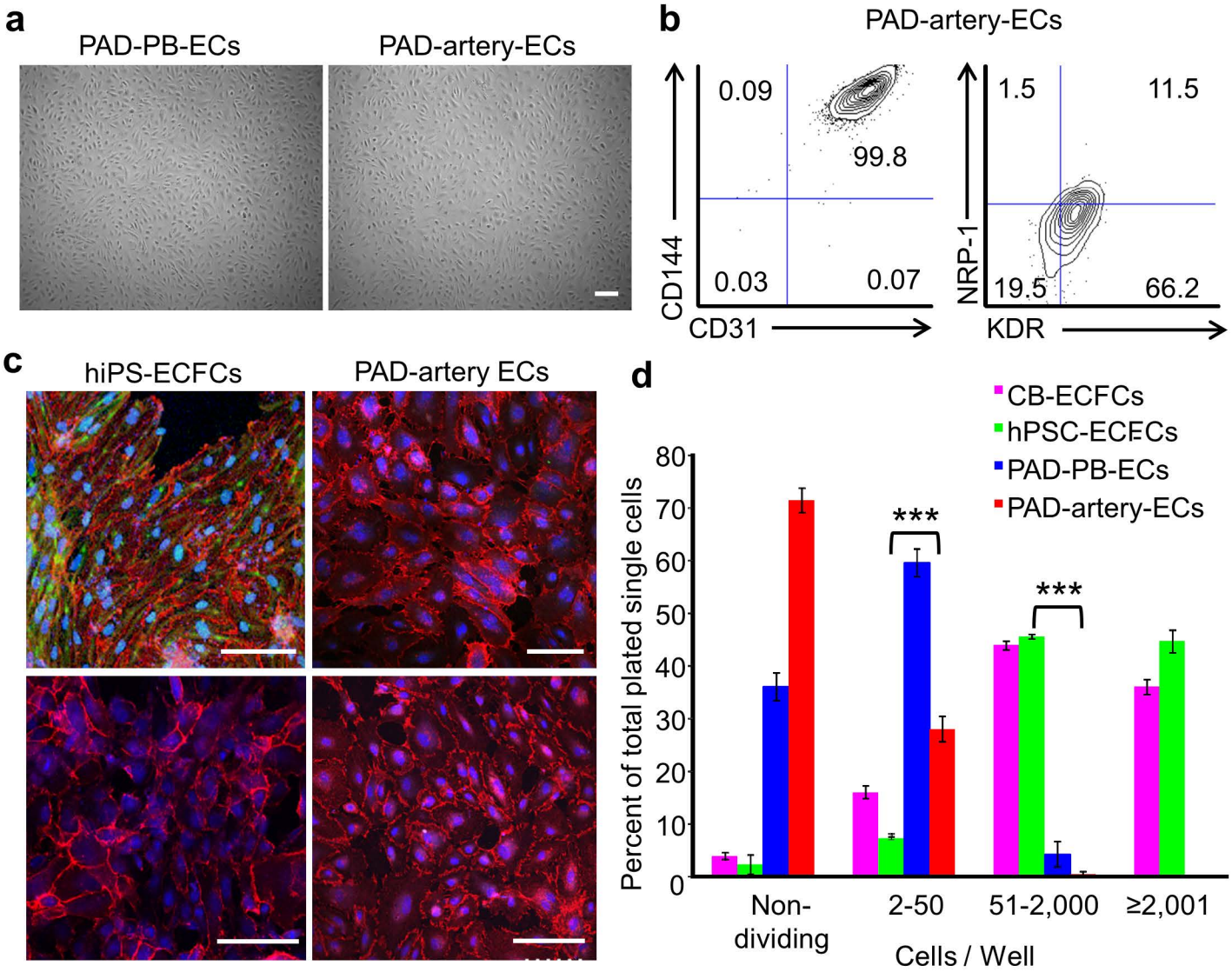

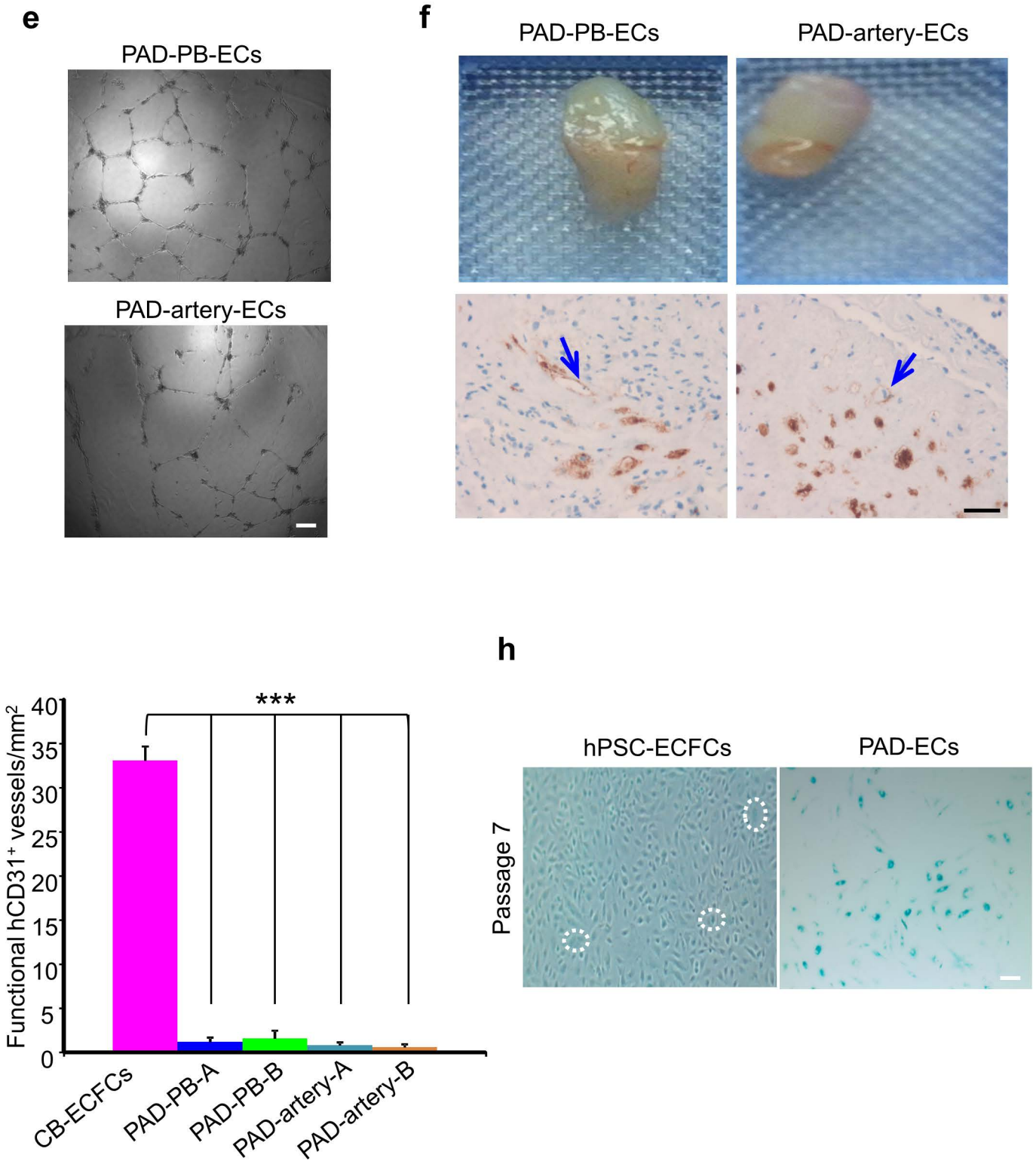
e
PAD-PB-ECs
PAD-artery-ECs
f
PAD-PB-ECs
PAD-artery-ECs
g
***
Functional hCD31+ vessels/mm2
40
35
30
25
20
15
10
5
0
CB-ECFCs
PAD-PB-A
PAD-PB-B
PAD-artery-A
PAD-artery-B
h
hPSC-ECFCs
PAD-ECs
Passage 7

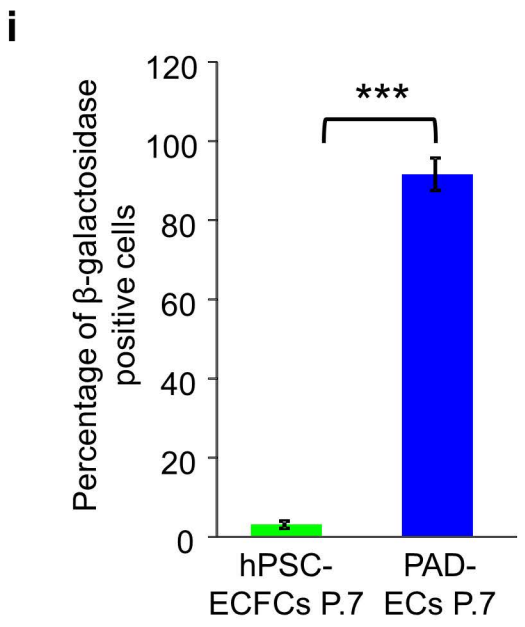
i
Percentage of β-galactosidase positive cells
120
100
80
60
40
20
0
***
hPSC-ECFCs P.7
PAD-ECs P.7

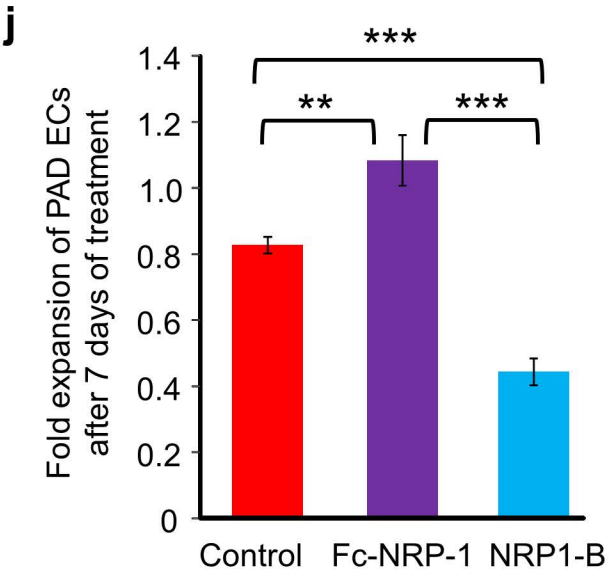
j
Fold expansion of PAD ECs after 7 days of treatment
1.4
1.2
1.0
0.8
0.6
0.4
0.2
0
***
**
***
Control
Fc-NRP-1
NRP1-B

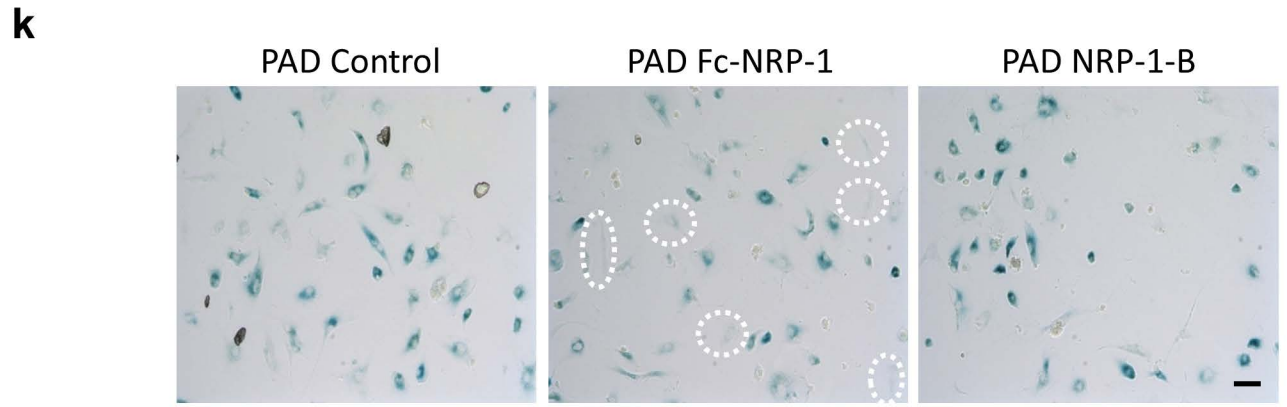
k
PAD Control
PAD Fc-NRP-1
PAD NRP-1-B

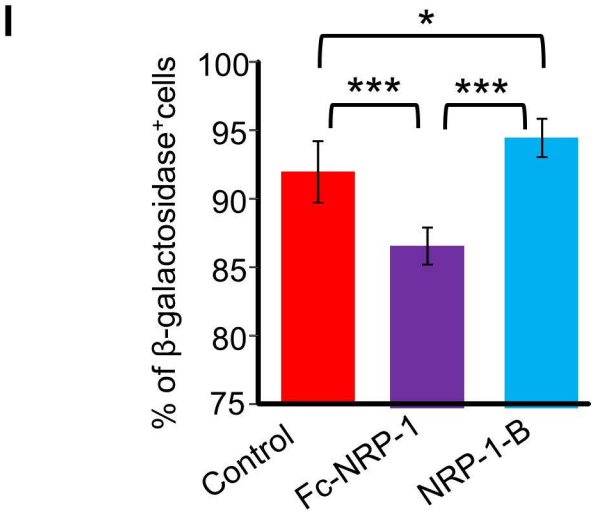
l
% of β-galactosidase+cells
100
95
90
85
80
75
*
***
***
Control
Fc-NRP-1
NRP-1-B

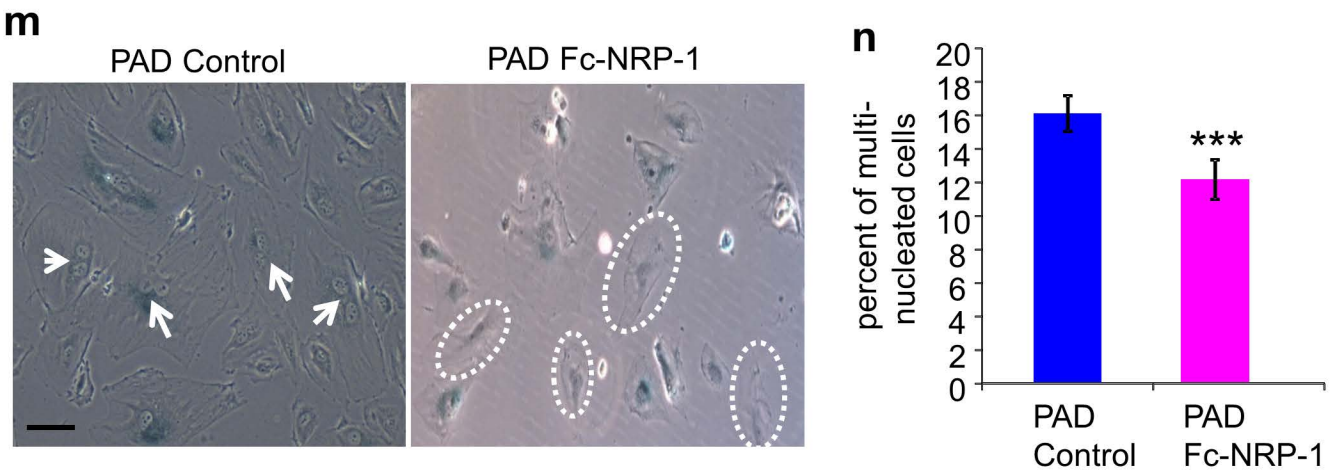

Supplementary Figure 8: PAD patients derived ECs possess diminished NRP-1 expression, undergo early cell senescence, fail to exhibit a complete hierarchy of clonal proliferative potential and have deficient *in vivo* vessel forming ability, however, exogenous NRP-1 treatment in PAD ECs decreases cell senescence, reduces multi nuclear cell formation and rescues PAD-EC proliferative potential. (a) Artery and peripheral blood ECs were derived from patients with peripheral vascular disease who underwent lower extremity amputations. A representative phase contrast photomicrographs indicates the homogenous characteristic cobblestone morphology of endothelial cells derived from PB (left panel) and artery (right panel) obtained from patients with PAD and CLI. All experiments were performed 6 times in duplicates and a representative photomicrograph is shown for each group. Scale bar, 50 μm. **(b)** ECs derived from PAD patients were subjected to flow cytometric analysis to determine expression of typical endothelial markers. PAD patient artery or PB derived endothelial cells were stained with monoclonal antibodies against human CD31, CD144, KDR and NRP-1. The percentage indicated in the upper right quadrant of contour plots indicates CD31 and CD144 double positive cells (left contour plot). Percentages in right contour plots indicate the percentage of cells co-expressing NRP-1 and KDR (upper right); NRP-1 expression (upper Left); KDR expression in lower right. While all of these cells maintained high levels of co-expression for CD31 and CD144 and more than 60% of the cells exhibited KDR expression, less than 11.5% of cells exhibited NRP-1 expression. All experiments were performed 5 times in triplicates and a representative contour plot is shown for each group. **(c)** Representative immunofluorescence micrographs of hiPS-ECFCs and PAD artery ECs indicating surface expression for endothelial markers CD31, CD144, NRP-1 and the non-endothelial marker α-SMA. In top panels, NRP-1 expression represented in green; CD31 expression represented in red. In bottom panels, α-SMA expression represented in green; CD144 expression represented in red. DAPI was used to stain the nucleus in blue. While hiPS-ECFCs exhibited NRP-1 and CD31 co-expression, stained positive for CD144 and completely lacked α-SMA expression, PAD-artery-ECs did not exhibit NRP-1 and CD31 co-expression, however, they did stain positive for CD31 and CD144, and completely lacked a-SMA expression. All experiments were performed 4 times in duplicates and a representative photomicrograph is shown for each group. Scale bars, 100 μm. **(d)** hiPS-ECFCs and ECs derived from PAD patients were subjected to single cell proliferative potential assay. Single cells from each of these groups were plated in 96-well plates and scored after 14 days of plating. Endothelial cells from PAD patients exhibited poor proliferative behavior as about 70% of resident vessel wall (artery) and more than 30% of PB derived endothelial cells remained as a single non dividing cell. In contrast only 2% of the single plated cells in CB-ECFCs and hiPS-ECFCs groups remained as non-dividing cells after 14 days of culture. Those PAD derived cells that divided mostly formed endothelial clusters (28% PAD-artery-ECs and 60% PAD-PB-ECs), few formed LPP-ECFC (0.5% PAD-artery-ECs and 4% PAD-PB-ECs) and none of them gave rise to HPP-ECFC. However, cells from CB-ECFCs and hiPS-ECFCs groups that divided formed few endothelial clusters and mostly formed LPP-ECFC (44.3% CB-ECFCs and 44.7% hiPS-ECFCs) and HPP-ECFC (35% CB-ECFCs and 43% hiPS-ECFCs). n = 3; Student's *t*-test: ***$p<0.001$.

(e) Representative phase contrast photomicrographs of PAD patient derived ECs from artery and peripheral blood demonstrating the ability to form capillary-like networks on Matrigel. All experiments were performed 5 times in duplicates and a representative photomicrograph is shown for each group. Scale bar, 100 μm. **(f)** ECs derived from PAD patients were implanted in immunodeficient mice. Gels were recovered after 14 days of implantation, fixed, permeabilized and stained with specific anti-human CD31 antibody that does not cross react with mouse host cells. Arrows indicated in a representative photomicrograph identify a few small anti-human $CD31^+$ blood vessels that are perfused with circulating host red blood cells. All experiments were performed 5 times in triplicates and a representative photomicrograph is shown for each group. Scale bar, 50 μm. **(g)** A bar graph represents quantification of functional $hCD31^+$ vessels counted per mm^2 in each group. ECs derived from PAD patients exhibited a significantly diminished number of functional $hCD31^+$ vessels compared to the CB-ECFC control. n ≥ 3; mean ± SD. Student's *t*-test: ***$p<0.001$. **(h)** PAD-ECs and hiPS-ECFCs (P7) were stained with β-galactosidase as per manufacturer instructions. Almost all cells were β-galactosidase positive blue cells in the PAD-EC group, whereas fewer cells were (indicated by circles) β-galactosidase positive in the hiPS-ECFCs group. All experiments were performed 4 times in triplicates and a representative photomicrograph is shown for each group. Scale bar, 50 μm. **(i)** A bar graph depicting the percentages of β-galactosidase positive PAD ECs compared to hiPS-ECFCs. A significantly higher percentage of β-galactosidase positive blue cells were observed in PAD-ECs compared to hiPS-ECFCs. n = 10; mean ± SD. Student's *t*-test: ***$p<0.001$. **(j)** PAD-artery ECs (P7) were treated with control, Fc-NRP-1 and NRP-1-B for 7 days. A bar graph represents fold expansion of PAD-artery ECs following 7 days of treatments with control, Fc-NRP-1 and NRP-1-B. While a significantly higher fold expansion was observed in Fc-NRP-1 treated group compared to control, a significantly decreased expansion was observed in NRP-1-B treated group compared to the control group. n = 3; mean ± SD. Student's *t*-test: **$p<0.01$ and ***$p<0.001$. **(k)** PAD-artery ECs (P7) were treated with control, Fc-NRP-1 and NRP-1-B for 7 days and were stained with β-galactosidase as per manufacturer's instruction. Almost all cells stained positive for β-galactosidase staining in the control and NRP-1-B treated groups, whereas some cells in the Fc-NRP-1 treated group did not stain positive for β-galactosidase staining (indicated by circles). All experiments were performed 4 times in triplicates and a representative photomicrograph is shown for each group. Scale bar, 50 μm. **(l)** A bar graph indicates the percentages of β-galactosidase positive cells following the treatment of PAD-artery endothelial cells with control, Fc-NRP-1 and NRP-1-B for 7 days. Significantly decreased β-galactosidase positive blue cells were observed in Fc-NRP-1 treated cells compared to control treated cells. n = 6; mean ± SD. Student's *t*-test: *$p<0.05$ and ***$p<0.001$. **(m)** PAD-artery ECs (P7) were treated with control and Fc-NRP-1 for 7 days and photomicrographs of the cells obtained to count nuclei numbers in treated cells. A representative photomicrograph with arrows indicating multinucleated blue cells in control (left panel) and circles indicating non-blue cells with a single nucleus (right panel). All experiments were performed 4 times in triplicates and a representative photomicrograph is shown for each group. Scale bar, 25 μm. **(n)** A bar graph indicates the percentage of multi-nucleated PAD ECs in control compared to Fc-NRP-1 treated cells. A significantly reduced percentage of multinucleated cells were observed in Fc-NRP-1 treated cells compared to control treated cells. n = 6; mean ± SD. Student's *t*-test: ***$p<0.001$.

Supplementary Figure 9: Full length western blots showing KDR, p130^{Cas} and Pyk2 phosphorylation.

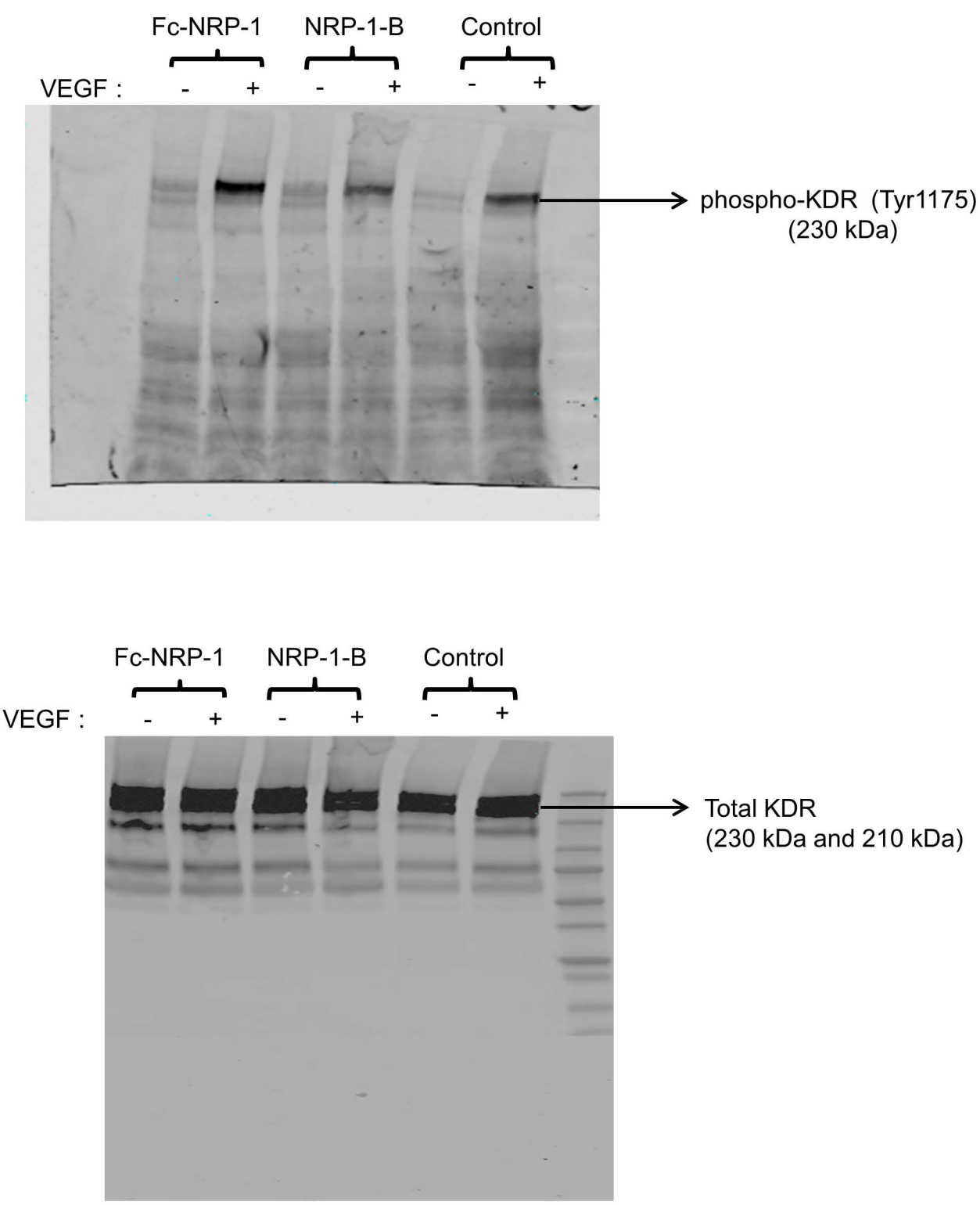

c

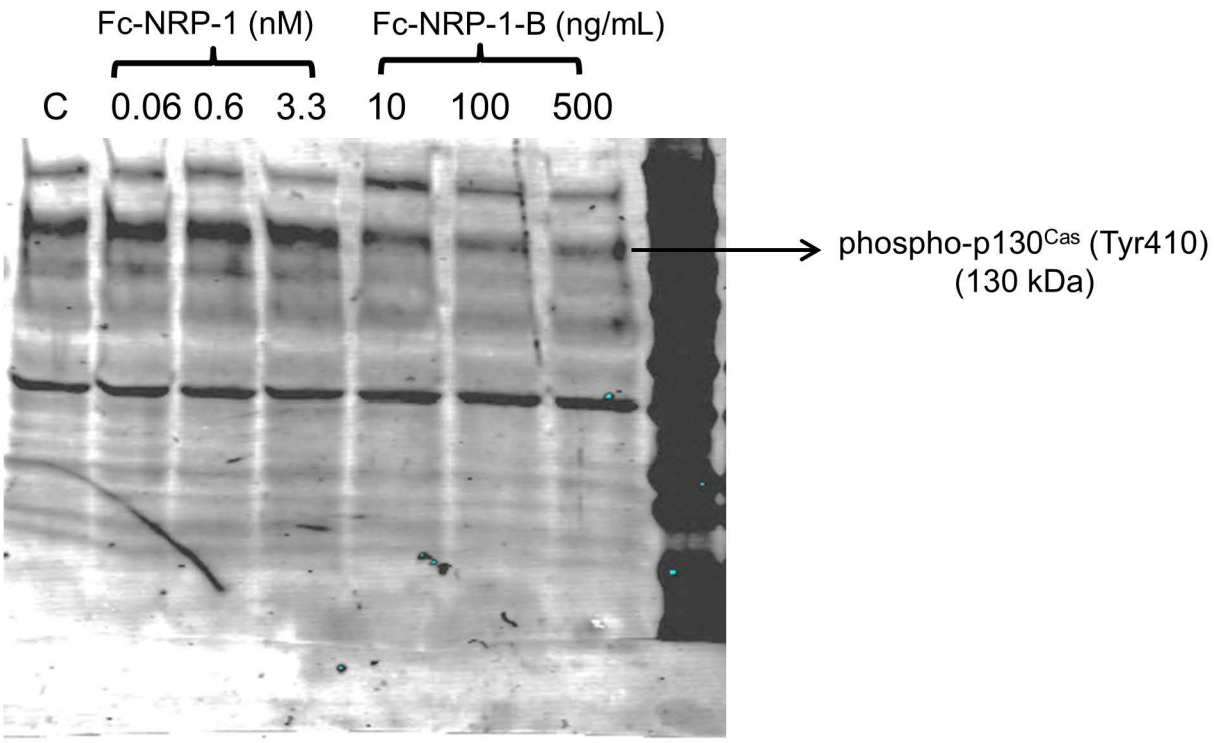
Fc-NRP-1 (nM)
Fc-NRP-1-B (ng/mL)
C
0.06
0.6
3.3
10
100
500
phospho-p130Cas (Tyr410)
(130 kDa)

d

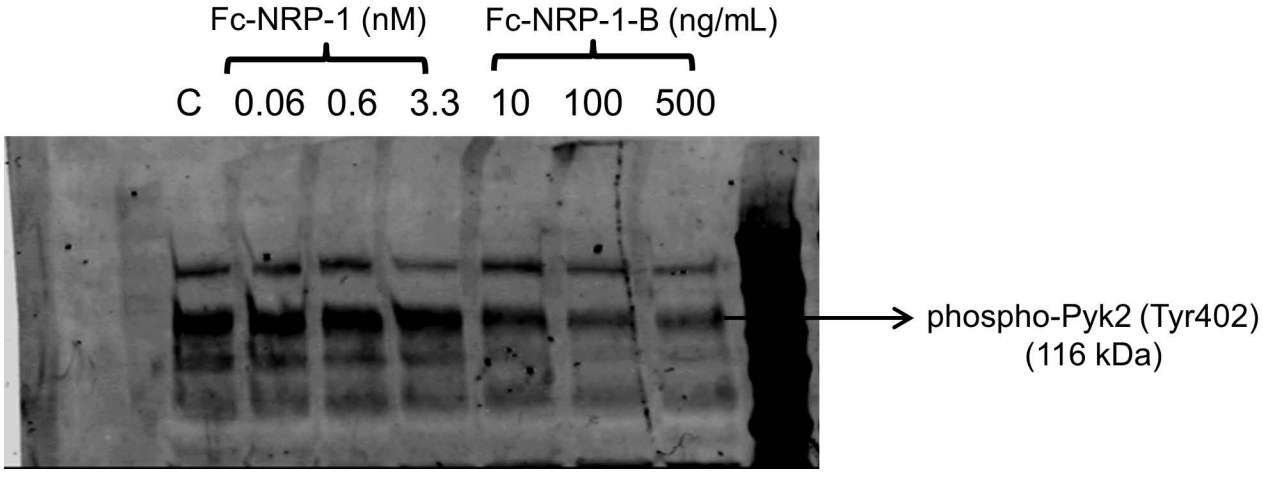
Fc-NRP-1 (nM)
Fc-NRP-1-B (ng/mL)
C
0.06
0.6
3.3
10
100
500
phospho-Pyk2 (Tyr402)
(116 kDa)

e

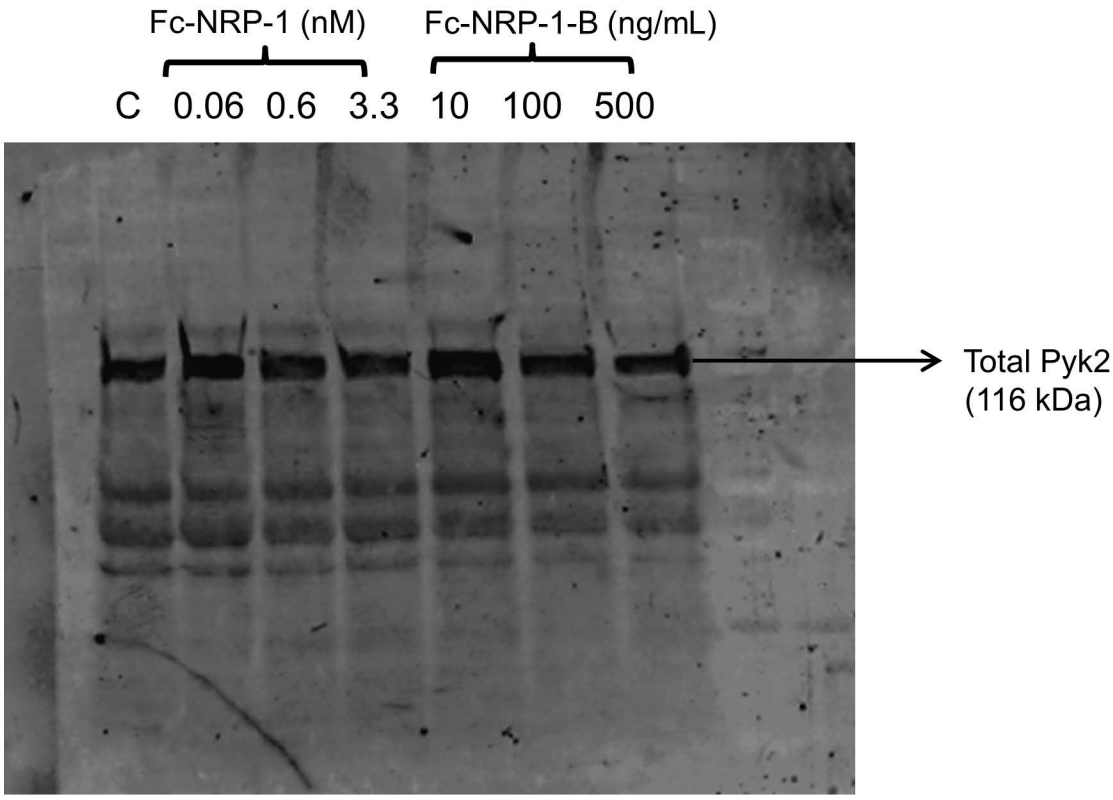

Supplementary Figure 9: Full length western blots showing KDR, p130^{Cas} and Pyk2 phosphorylation. Western blots were prepared as described in Methods and in Fig. 3c. Blot **a** was first prepared with phospho-KDR antibody and was stripped to incubate with total KDR antibody (blot **b**). Similarly, blot **c** was first prepared with phospho-p130^{Cas} and was subsequently stripped twice to re-incubate with phospho-Pyk2 (blot **d**) and total phospho-Pyk2 (blot **e**) antibodies.

Supplementary Table 1 : List and description of human pluripotent stem cell lines used in the studies.

Cell line	Description
DF19-9-11T	Induced pluripotent stem cells reprogrammed from human foreskin fibroblasts using nonintegrating episomal vectors[16].
FCB-iPS-1	Induced pluripotent stem cells reprogrammed from frozen human cord blood derived $CD34^+$ cells using lentiviral vectors[13].
FCB-iPS-2	Induced pluripotent stem cells reprogrammed from frozen human cord blood derived $CD34^+$ cells using lentiviral vectors[13].
H9	Human embryonic stem cell line derived from the inner cell mass of a blastocyst-stage embryo[15].

Supplementary Table 2 : Supplementary Table 2: Flow, Western blot, Immunohistochemical and Immunofluorescence Staining Antibodies.

Name of the reagent	Company	Host species	Catalogue number	Clone number	Dilution factor
CD31, FITC conjugated (flow)	BD Pharmingen	Mouse	555445	WM59	5 µL / test (1 x 10^6 cells in 100 µL buffer)
CD31, PE-Cy7 conjugated (flow)	eBioscience	Mouse	25-0319-41	WM59	5 µL / test (1 x 10^6 cells in 100 µL buffer)
CD31 (immunofluorescence staining)	Dako	Mouse	IR610	JC70A	1:200
CD31 (immunohistochemistry)	Dako	Mouse	M082301-2	JC70/A	1:100
NRP-1, APC conjugated (flow)	Miltenyi Biotech	Mouse	130-090-900	AD5-17F6	10 µL / test (1 x 10^6 cells in 100 µL buffer)
NRP-1, PE conjugated (flow)	Miltenyi Biotech	Mouse	130-090-533	AD5-17F6	10 µL / test (1 x 10^6 cells in 100 µL buffer)
NRP-1 (immunofluorescence staining)	Santa Cruz	Rabbit	5541	H-286	1:100
CD144, PE conjugated (flow)	eBioscience	Mouse	12-1449-82	16B1	5 µL / test (1 x 10^6 cells in 100 µL buffer)
CD144, APC conjugated (flow)	eBioscience	Mouse	17-1449-42	16B1	5 µL / test (1 x 10^6 cells in 100 µL buffer)
CD144, purified (immunofluorescence staining)	eBioscience	Mouse	14-1449-82	16B1	1:200
KDR, PE conjugated	R&D Systems	Mouse	FAB357P	89106	10 µL / test (1 x 10^6 cells in 100 µL buffer)
hCD146, PE conjugated	BD Pharmingen	Mouse	550315		5 µL / test (1 x 10^6 cells in 100 µL buffer)
Phospho-VEGF Receptor 2 (Tyr1175)	Cell Signaling	Rabbit	2478	19A10	1:1000
VEGF Receptor 2	Cell Signaling	Rabbit	2479	55B11	1:1000
Phospho-p130 Cas (Tyr410)	Cell Signaling	Rabbit	4011	N/A	1:1000
Phospho-Pyk2 (Tyr402)	Cell Signaling	Rabbit	3291	N/A	1:1000
Pyk2	Cell Signaling	Rabbit	3292	N/A	1:1000
a-SMA	Dako	Mouse	M0851	1A4	1:200
DAPI	Molecular Probe	N/A	P36935	N/A	1 drop
Annexin V Apoptosis Detection Kit APC	eBioscience	N/A	88-8007-72	N/A	2.5 µL / test (1 x 10^6 cells in 100 µL buffer)